ORIGINAL ARTICLE

Preparation of nano-Co₃O₄-coated *Albizia procera*-derived carbon by direct thermal decomposition method for electrochemical water oxidation

Ismail A. Buliyaminu [a,b], Md. Abdul Aziz [b,*], Syed Shaheen Shah [a,b],
A.K. Mohamedkhair [a,b], Zain H. Yamani [a,b]

[a] *Physics Department, King Fahd University of Petroleum and Minerals, Dhahran 31261, Saudi Arabia*
[b] *Center of Research Excellence in Nanotechnology (CENT), King Fahd University of Petroleum and Minerals, KFUPM Box 5040, Dhahran 31261, Saudi Arabia*

Abstract It is obtained that nano-Co₃O₄-coated carbon prepared by thermal decomposition of Co(NO₃)₂·6H₂O at 300 °C on home-made *Albizia procera (Roxb.)* leaves derived carbon is an efficient electrocatalyst for electrochemical water oxidation in 0.1 M NaOH (aq.) solution. The loading of nano-Co₃O₄ on the carbon was changed by varying the amount of precursor of cobalt (100–1000 mg) and using a constant amount of the carbon (200 mg) during thermal decomposition. The prepared samples were characterized by physical techniques, including X-ray diffraction (XRD), field emission scanning electron microscopy (FESEM), energy dispersive spectroscopy (EDS), thermo-gravimetric analysis (TGA), fourier transform infrared spectroscopy (FTIR), high-resolution transmission electron microscopy (HRTEM), diffuse reflectance spectroscopy (DRS), Brunauer-Emmett-Teller (BET) and X-ray photoelectron spectroscopy (XPS). XRD, TEM, FESEM, and EDS confirmed the formation of uniformly distributed nanoparticles of single-phase Co₃O₄ on the surface of carbon. The XRD data reveals formation of nano-Co₃O₄ with average particle sizes in the range of 9–17 nm. The FESEM micrographs demonstrate that Co₃O₄ nanoparticles, having irregular morphology, are uniformly and densely covered on the surface of supporting carbon.. The prepared samples were immobilized on the filter paper derived carbon electrode (FPCE) to study their electrocatalytic properties toward water oxidation. The cyclic voltammetric studies showed that the nano-Co₃O₄-C prepared using 400 mg of Co(NO₃)₂·6H₂O (nano-Co₃O₄-C-400), which possesses meso- and macropores with BET surface area of 192.4 m²/g, reaches a current density of 28 mAcm⁻² at 1.5 V and electrochemical water oxidation starting potential of

* Corresponding author.
E-mail address: maziz@kfupm.edu.sa (M.A. Aziz).

0.7 V. In this work, it is also shown that the current densities, at 1.5 V, increase by increasing the amount of cobalt oxide in the prepared samples though. The nano-Co_3O_4-C-400 catalyst shows optimum performance for electrochemical water oxidation in terms of starting water oxidation potential, reasonable amount of Co_3O_4 and moderate level of current density at 1.5 V.

1. Introduction

The current resources of energy are insufficient to fulfill the future demands of global energy (Asif and Muneer, 2007). Therefore, novel technological developments to utilize sustainable, clean, and viable energy resources are highly needed (Chu and Majumdar, 2012; Dragunov et al., 2018; Turner et al., 1999; Zotov et al., 2017). Among the available resources of energy, hydrogen gas (H_2) is one of the emerging energy carriers, but generally nature exist hydrogen cannot generate energy due to its low concentration. To generate enough amount of hydrogen to produce energy, electrochemical water (H_2O) splitting could be an option. Here, H_2O could undergo electrochemical splitting to produce green fuel in the form of hydrogen gas (Jiao et al., 2015; Züttel et al., 2010). However, the efficiency of such hydrogen generation significantly depends on favorable catalysts to promote the hydrogen evolution reaction (HER) and achieve fast kinetics in practical applications. During the past few decades, several heterogeneous and molecular catalysts (Blakemore et al., 2015; McCrory et al., 2013; Zhang et al., 2016) have been produced to accomplish water oxidation at lower overpotential. In particular, earth-abundant metal catalysts (Hunter et al., 2016; Roger et al., 2017) could possibly substitute the Ru, Pt, and Ir based benchmark oxygen evolution reaction (OER) catalysts (Reier et al., 2012). Amongst the abundantly available transition metals, much attention has been concerted on cobalt, since the pioneer work of Nocera (Kanan and Nocera, 2008). Indeed, several catalysts based on chalcogenides, phosphides, phosphates, and oxides of cobalt have been developed for water splitting (Deng and Tüysüz, 2014; Gerken et al., 2011; J. Wang et al., 2016).

The nano-sized transition metal oxides, including Co_3O_4, TiO_2, Fe_2O_3, CuO and NiO, have attracted much research interest due to their unique electrochemical, electronics, chemical and physical properties (Fernández-García et al., 2004; Khomane et al., 2008). Specifically, research has been conducted using nano-Co_3O_4 for various applications such as electrochemical water splitting (Chen et al., 2015), electrochemical gas sensing (Guo et al., 2013; Jia et al., 2009; Xu and Cheng, 2016), fuel cells (Babar et al., 2018), solar cells (Kabre et al., 2011; Sharma et al., 2015), supercapacitors (X. Wang et al., 2016), catalysis (Ma, 2014; Sharma et al., 2015), and batteries (Su et al., 2014).

Due to its indispensable wide range of applications, several approaches have been developed to synthesize nano-Co_3O_4 materials with various morphologies, sizes, and shapes (Ahmed Qasem et al., 2017; Fernández-García et al., 2004; Harish et al., 2016; Luisetto et al., 2008; Qasem et al., 2019; Xu and Zeng, 2003; Zhou et al., 2013). Among the numerous approaches developed to prepare nano-Co_3O_4, thermal decomposition method has been reported as one of the simple,

time effective, and promising methods (Ahmed Qasem et al., 2017).

For preparing nano-Co_3O_4 material using thermal decomposition method, a suitable cobalt precursor is required. Among the reported cobalt precursors are cobalt hydroxide decomposed at 500 °C (Mahmoud and Al-Agel, 2011), cobalt malonate (Bhattacharjee et al., 2013a), cobalt oxalate rods (Ahmed et al., 2008), cobalt in plant extracts (Aspalathus linearis) (Xu and Zeng, 2003), cobalt-citrate (Raman et al., 2016), cobalt (II)-tartrate complex (Bhattacharjee et al., 2013b), and cobalt hydroxyl carbonates (Diallo et al., 2015). Most of these precursors require pre-reaction, making it tedious and time consuming. So, it would be better to employ a simple and straightforward method to prepare pure nano-Co_3O_4 through a thermal decomposition of an abundant cobalt inorganic precursor such as $Co(NO_3)_2·6H_2O$. Qasem et al. (2019) reported a simple and direct thermal decomposition of $Co(NO_3)_2.6H_2O$ at 520 °C to prepare pure nano-Co_3O_4 in the air atmosphere without any pre-reaction.

As reported by the scientific community (Bajdich et al., 2013; Deng and Tüysüz, 2014; Gerken et al., 2011), cobalt oxide is one of the suitable catalysts for electrochemical water oxidation. Particularly, the cobalt oxide can electrooxidize water to O_2 at basic pH selectively (Gerken et al., 2011). But as there are limited resources of metals (especially cobalt) in the world, which restrict their practical applications in O_2 evolution reactions. Therefore, to preserve metals (cobalt), it would be better if we can coat cobalt oxide on some cheap scaffolder, like biomass derived carbon and to achieve similar performance for electrochemical water oxidation. Though, several carbon materials such as carbon nanotube (SWCNT or MWCNT), mesoporous carbon and graphene have been extensively reported as conductive substrates, due to their high conductivity and specific surface area (Liang et al., 2012; Wu et al., 2012), yet they are all relatively expensive.

Herein, we employ the direct thermal decomposition of $Co(NO_3)_2·6H_2O$ at 300 °C without any pre-reaction, not only to prepare pure nano-Co_3O_4, but also coated it on home-made carbon (Albizia procera derived carbon). The idea of combining nano-Co_3O_4 with carbon substrate comes to save cobalt and to improve the catalytic properties, including activity and stability. The home-made carbon coated with nano-Co_3O_4 demonstrates a decent activity and has gained the author attention as a catalyst for electrochemical water oxidation.

2. Experimental

2.1. Materials and method

All chemical reagents including cobalt (II) nitrate hexahydrate $Co(NO_3)_2·6H_2O$ (ACS reagent, ≥98%) and sodium hydroxide

NaOH (ACS reagent, ≥97.0%) were used directly as purchased from Sigma-Aldrich (*http://www.sigmaaldrich.com*) without any further purification. Filter papers were purchased from Whatman. Copper tape (one-sided adhesive) and scotch tape-898 (one-sided adhesive) premium grade were both obtained from 3 M, United states.

Initially, the carbon was prepared by pyrolysis of dried powder (≤100 μm) of *Albizia procera* (Roxb.) leaves at 800 °C. The details of the preparation will be summarized in somewhere else. The preparation of nano-Co$_3$O$_4$ on this home-made carbon (nano-Co$_3$O$_4$-C) is illustrated in Fig. 1 and tabulated in Table 1. Initially, 100 mg of Co(NO$_3$)$_2$·6H$_2$O and 200 mg of *Albizia procera* (Roxb.) leaves derived carbon were added directly into 100 mL of de-ionized (DI) water in two separate beakers and ultrasonicated using sonicator (Bransonic Ultrasonic cleanser: 5510E-DTH) for one hour to prevent particles from aggregation. The two separate solutions were mixed together and sonicated at room temperature for 40 min. The resultant mixture was heat treated at 110 °C for one hour under rigorous stirring (at 300 rpm) to remove the water. Afterward, the mixture was dried overnight in an electric oven at 60 °C. The final dried mixture was transferred to a boat type alumina crucible and thermally decomposed at 300 °C for 180 min in an electric tube furnace (OTF-1200X-S/www.mtixtl.com (USA)) to obtain nano-Co$_3$O$_4$-C. Initially, the temperature was increased at heating rate of 10 °C/min from the room temperature, to a maximum temperature of 300 °C, which was later maintained for 180 min. At the elevated temperature, Co(NO$_3$)$_2$·6H$_2$O-C was decomposed to nano-Co$_3$O$_4$-C through the formation of Co(NO$_3$)$_2$·4H$_2$O-C, Co(NO$_3$)$_2$·2H$_2$O-C, Co(NO$_3$)$_2$·H$_2$O-C, Co(NO$_3$)$_2$-C, CoOOH-C and Co$_2$O$_3$-C intermediate compounds (Aslan et al., 2019). Next, the temperature was decreased at cooling rate of 5 °C/min from 300 °C to the room temperature. The nano-Co$_3$O$_4$-C obtained by using 100 mg Co(NO$_3$)$_2$·6H$_2$O is denoted as nano-Co$_3$O$_4$-C-100 in rest of this manuscript. The procedure was repeated for 200, 400, 600, 800 and 1000 mg of precursor to obtain nano-Co$_3$O$_4$-C-200, nano-Co$_3$O$_4$-C-400, nano-Co$_3$O$_4$-C-600, nano-Co$_3$O$_4$-C-800 and nano-

Table 1 List of prepared samples using different amount of Co(NO$_3$)$_2$·6H$_2$O with constant amount of carbon, investigated in the present study.

S. No.	Carbon mass (mg)	Co(NO$_3$)$_2$·6H$_2$O mass (mg)	Name of the samples
1	200	100	Nano-Co$_3$O$_4$-C-100
2	200	200	Nano-Co$_3$O$_4$-C-200
3	200	400	Nano-Co$_3$O$_4$-C-400
4	200	600	Nano-Co$_3$O$_4$-C-600
5	200	800	Nano-Co$_3$O$_4$-C-800
6	200	1000	Nano-Co$_3$O$_4$-C-1000

Co$_3$O$_4$-C-1000, respectively. The idea here is to study the effect of increasing amount of precursor on water oxidation catalytic properties including activity and stability.

2.2. Materials characterization

The X-ray diffraction (XRD) patterns of nano-Co$_3$O$_4$-C-100, 200, 400, 600, 800, and 1000 samples were recorded at a scan rate of 1.00° per min in the 2θ-range from 5° to 80° by a Rigaku Miniflex II diffractometer equipped with Cu K-alpha radiation. The morphological properties of the prepared samples were obtained using a scanning electron microscope (Tescan Lyra-3). The energy dispersive X-ray spectroscopy (EDS) spectra were recorded on a Lyra 3 attachment to the FESEM using LINK INCA program system. Further morphological and diffraction properties of the synthesized nano-Co$_3$O$_4$-C-400 sample was obtained using a transmission electron microscope (JEOL JEM 2100F). Thermogravimetric Analysis (TGA) was carried out by heating 16 mg of nano-Co$_3$O$_4$-C-400 from 30 °C to 1000 °C at a heating rate of 10 °C/min in the nitrogen atmosphere. An X-ray photoelectron spectrometer (XPS) (ESCALAB 250Xi XPS Microprobe, Thermo Scientific, USA) was applied for chemical analysis of the prepared samples. The band gap of nano-Co$_3$O$_4$-C-400 was calculated
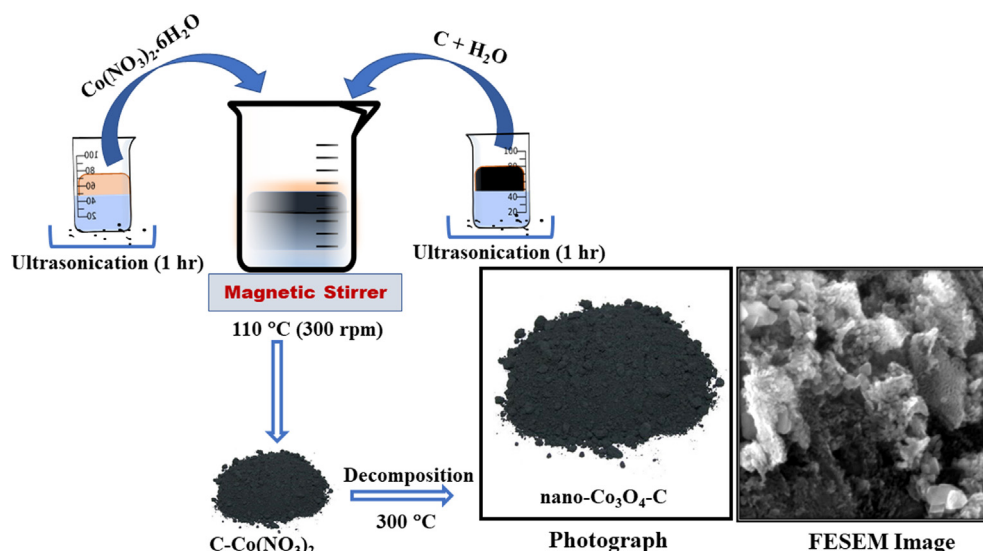

Fig. 1 Schematic representation for the preparation of nano-Co$_3$O$_4$-C.

using a Cary 5000 high performance UV–Vis-NIR spectrophotometer with photometric performance in the range of 175–3300 nm, equipped with diffuse reflectance spectrometer. Fourier transform infrared spectroscopy (FTIR) was carried out using Thermo Scientific NICOLET 6700 spectrometer, and the spectra were obtained in the range of 4000–500 cm^{-1} with 32 scans per spectrum and 4 cm^{-1} resolution.

2.3. Electrode fabrication

The filter paper derived carbon electrode (FPCE) was prepared using a pyrolysis process by cutting filter papers into pieces of 2 cm by 2 cm area. These pieces of filter papers were placed in an alumina flat bottom boat shaped crucible, which was later inserted into a cylindrical alumina tube with both ends of the tube sealed. Nitrogen gas was passed through one end for about 5 min to flush out oxygen and the moisture from the tubular furnace. The sized filter papers were heated at 850 °C for 5 h in the presence of nitrogen atmosphere. The resulting FPCE were fixed with scotch and copper tapes, as shown in Fig. 2(a). The entire surface area of FPCE was covered except a 0.2 cm^2 area which serves as a substrate for the working electrode. To prepare the working electrode nano-Co_3O_4-C/FPCE, a solution of 10 mg of the prepared nano-Co_3O_4-C was made in 5 mL of DI water which was sonicated for 5 min. 30 μL volume of the dispersed solution was immobilized on the exposed 0.2 cm^2 area using a drop and drying method, at room temperature. To assess the water oxidation catalytic activity of the nanostructured composites in alkaline condition ($2OH^- \rightarrow O_2 + 2H^+ + 4e^-$), the prepared working electrodes were tested as a selective oxygen evolving anode shown in Fig. 2(b).

2.4. Electrochemical measurement

The electrochemical measurements were performed using a CHI (760E) electrochemical workstation. The prepared nano-Co_3O_4-C/FPCE was used as the working electrode for electrochemical water oxidation in 0.1 M of NaOH (aq.) at room temperature. Ag/AgCl and platinum wire were used as the reference electrode and the counter electrode respectively, to complete the three-electrode cell.

3. Results and discussion

3.1. XRD analysis of nano-Co_3O_4-C

The X-ray diffraction (XRD) patterns of all the prepared samples were obtained to study the effect of different amount of $Co(NO_3)_2 \cdot 6H_2O$ precursor on the crystalline and phase structures of nano-Co_3O_4-C. The XRD patterns obtained for nano-Co_3O_4-C-100, nano-Co_3O_4-C-200, nano-Co_3O_4-C-400, nano-Co_3O_4-C-600, nano-Co_3O_4-C-800, and nano-Co_3O_4-C-1000 are shown in Fig. 3. The diffraction peaks for all the samples are identical which shows that all the prepared samples exhibit crystalline states and display the same phase. The major peaks in each pattern occurred at 2θ values of 19.1°, 25.2°, 31.4°, 36.9°, 44.8°, 59.4° and 65.2° which correspond to 111, 220, 311, 400, 422, 511, and 440 planes of face centered cubic nano-Co_3O_4 crystal according to JCPDS database (JCPDS 42-1467) (Kang and Zhou, 2015). The unidentified peak in between 22° to 30° is related to carbon. We calculated crystallite sizes of the prepared nano-Co_3O_4 on C using Debye-Scherrer formula (Zsigmondy and Scherrer, 1912) (Eq. (1)):

$$D = \frac{K\lambda}{\beta\cos\theta} \tag{1}$$

where, for Cu K-alpha, λ = 1.5406 Å and K (is a Scherrer's constant) ~ 0.9. The value of β was calculated from the value of the full width at half maximum (FWHM) by choosing the most intensive peak, 2θ = 36.9° for the (3 1 1) planes. Therefore, the calculated crystallite sizes of the prepared nano-Co_3O_4-C were found to be 9.4, 9.5, 9.7, 17.2, 15.9 and 15.5 nm for nano-Co_3O_4-C-100, nano-Co_3O_4-C-200, nano-Co_3O_4-C-400, nano-Co_3O_4-C-600, nano-Co_3O_4-C-800 and nano-Co_3O_4-C-1000, respectively. Besides, the crystallinity of

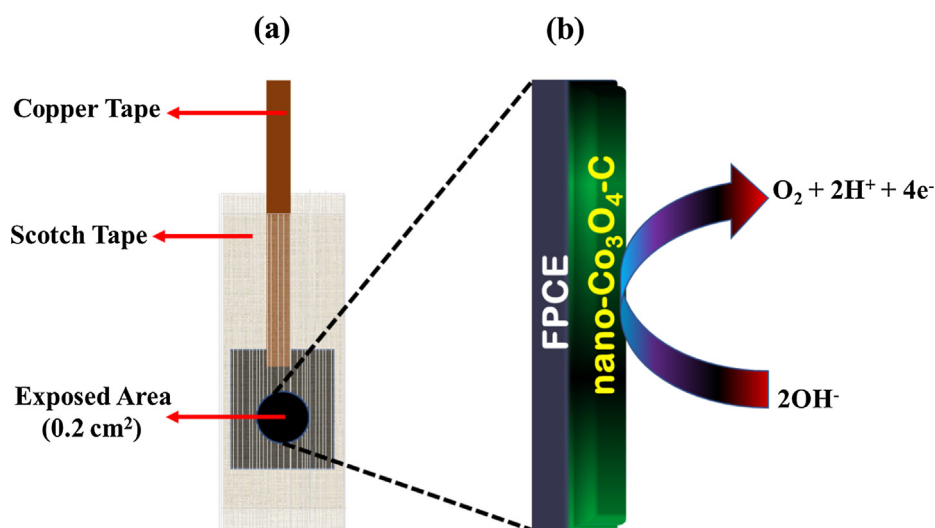**Fig. 2** Schematic (a) of the FPCE and (b) representation for a water-splitting electrocatalytic activity on an integrated nano-Co_3O_4-C/FPCE oxygen-evolving anode.

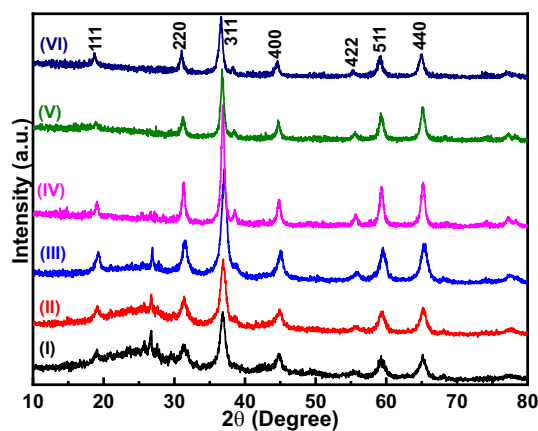**Fig. 3** XRD patterns of (I) nano-Co$_3$O$_4$-C-100, (II) nano-Co$_3$O$_4$-C-200, (III) nano-Co$_3$O$_4$-C-400, (IV) nano-Co$_3$O$_4$-C-600, (V) nano-Co$_3$O$_4$-C-800, and (VI) nano-Co$_3$O$_4$-C-1000.

the prepared nano-Co$_3$O$_4$-C has been increased with increasing the amount of cobalt precursor from 100 to 600 mg as per highest crystal plane peak (3 1 1). However, further increasing the cobalt precursor decreases the crystallinity gradually.

3.2. Morphological and compositional characterization of nano-Co$_3$O$_4$-C

The morphological and compositional details of the as-prepared nano-Co$_3$O$_4$-C samples were characterized by FESEM and EDS measurements. In Fig. 4(A–F), the high magnification FESEM images of nano-Co$_3$O$_4$-C-100, nano-Co$_3$O$_4$-C-200, nano-Co$_3$O$_4$-C-400, nano-Co$_3$O$_4$-C-600, nano-Co$_3$O$_4$-C-800 and nano-Co$_3$O$_4$-C-1000 are shown. A careful inspection of these micrographs demonstrates that nano-Co$_3$O$_4$ nanoparticles are uniformly distributed on the surface

of the supporting carbon in all the prepared samples (Fig. 4 (A–F)). It can be seen that the particles adopt irregular morphology with different sized particles, but it is obvious that nano-Co$_3$O$_4$ were uniformly and densely covered on the surface of carbon after the thermal decomposition process. The SEM micrograph of nano-Co$_3$O$_4$-C-100 is presented in Fig. 4 (A). It is noted that the surface of the pure carbon is relatively smooth, which is reported in our earlier paper (Shah et al., 2019). The SEM images (Fig. 4(A)) shows that the surface of nano-Co$_3$O$_4$ modified carbon is relatively rough, which indicates the presence of nano-Co$_3$O$_4$ on the carbon surface. It is also observed that the nano-Co$_3$O$_4$ is uniformly distributed all over the carbon surface (Fig. 4(A–C)). While the other FESEM micrographs suggest that higher concentrations of the cobalt precursor resulted in the formation of more nanoparticles, leading to agglomeration. There is some agglomeration of particles in nano-Co$_3$O$_4$-C-600, nano-Co$_3$O$_4$-C-800, and nano-Co$_3$O$_4$-C-1000, which can decrease the electrochemical activity for water oxidation. However, in Fig. 4(A–C), the uniform dispersion of nano-Co$_3$O$_4$-C-100, nano-Co$_3$O$_4$-C-200 and nano-Co$_3$O$_4$-C-400 is evident, which provide an effective path for electrochemical water oxidation.

The elemental composition and purity of the prepared nano-Co$_3$O$_4$-C were analyzed by energy dispersive X-ray analyses. Several small and large areas of the nano-Co$_3$O$_4$-C-100, nano-Co$_3$O$_4$-C-200, nano-Co$_3$O$_4$-C-400, nano-Co$_3$O$_4$-C-600, nano-Co$_3$O$_4$-C-800, and nano-Co$_3$O$_4$-C-1000 were examined by EDS. As expected, the entire samples show the presence of cobalt Co, oxygen O, and carbon C. For example, the EDS spectra of nano-Co$_3$O$_4$-C-400 are displayed in Fig. 5 (A). The presence of some extra elements like Ca and Si in the EDS spectra might be due to the impurities of the carbon which was prepared from natural plants. EDS was also used to map the distribution of carbon, cobalt, and oxygen in the prepared nano-Co$_3$O$_4$-C-400. A visualization of the uniform distribution of cobalt, oxygen and carbon over the surface of
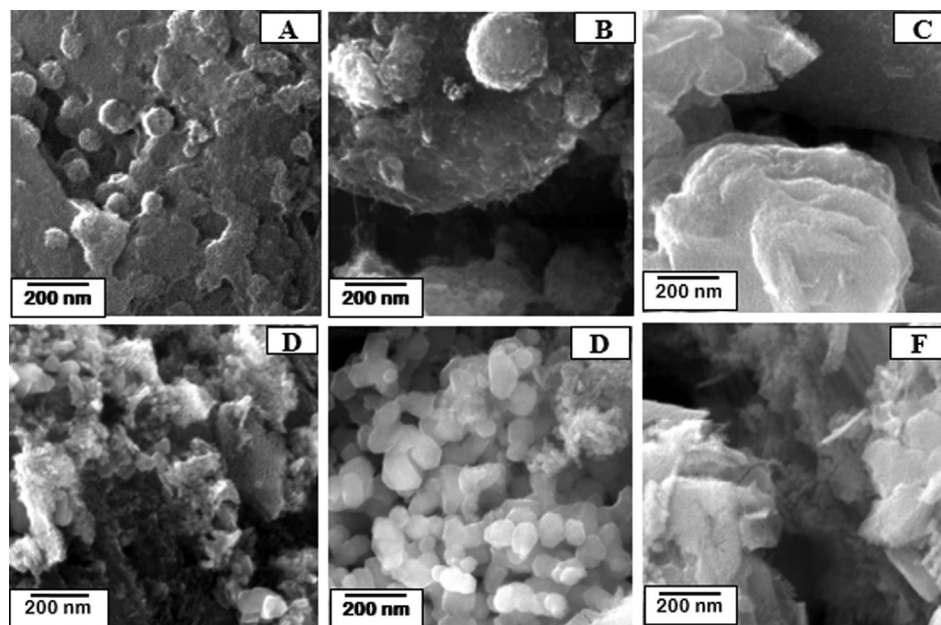

Fig. 4 FESEM images of (A) nano-Co$_3$O$_4$-C-100, (B) nano-Co$_3$O$_4$-C-200, (C) nano-Co$_3$O$_4$-C-400, (D) nano-Co$_3$O$_4$-C-600, (E) nano-Co$_3$O$_4$-C-800, and (F) nano-Co$_3$O$_4$-C-1000.
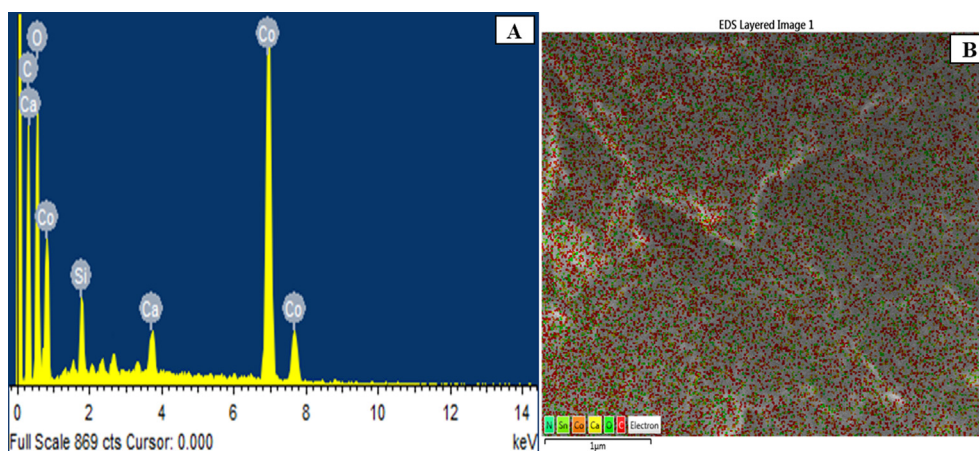
Fig. 5   (A) EDS spectrum and (B) Elemental mapping of nano-Co_3O_4-C-400.

the sample is given in Fig. 5(B). The other samples show similarly uniform elemental distributions

3.3. Transmission electron microscopy (TEM) of nano-Co_3O_4-C

Further analysis of nano-Co_3O_4-C-400 sample (optimum electrocatalyst, which has been described later of this manuscript) was performed using TEM. It is shown in Fig. 6 (a and b) that Co_3O_4 sample is composed of well dispersed and uniformed nano-structured particles with average particle size of 11.0 nm, which is closed to diameter obtained by XRD analysis (9.7 nm) . The related high-resolution transmission electron microscopy (HRTEM) image (Fig. 6(c)) shows the aligned lattice fringes with d spacing of 0.28 nm correspond to the (2 2 0) plane of cubic Co_3O_4 (Yu et al., 2013) which is one of the identified crystal plane of our prepared Co_3O_4 -C by XRD analysis

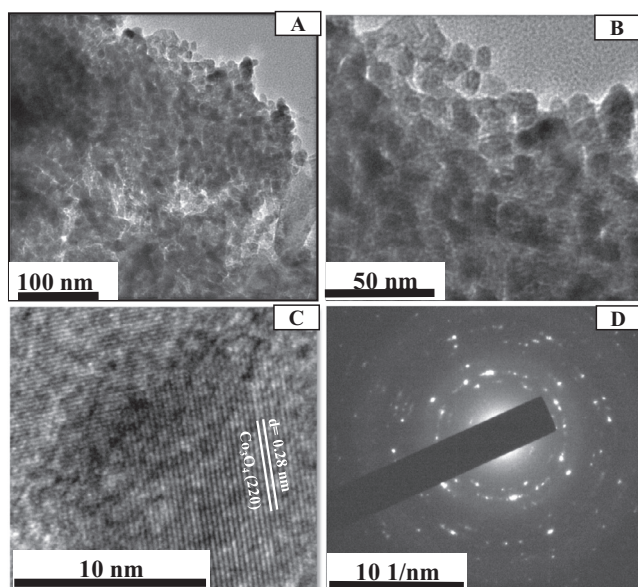(Fig. 3). The selected area electron diffraction (SAED) rings, shown in Fig. 6(d), confirms the polycrystalline nature of Co_3O_4 and agrees with the crystal planes presented in the XRD data (Bergmann et al., 2015).

3.4. Thermogravimetric analysis of nano-Co_3O_4-C

The thermogravimetric analysis (TGA) of nano-Co_3O_4-C-400 was carried out at a heating rate of 10 °C/minutes from 30 °C to 1000 °C in ambient atmosphere. The TGA curve in Fig. 7 revealed that the first mass loss occurred upon heating from 40 °C to 100 °C, at this point ~10% of the original weight of nano-Co_3O_4-C-400 was lost. This mass loss relates to removal of moisture from nano-Co_3O_4-C-400. The second observation of a sharp mass loss occurred when temperature is increased from 320 °C to 450 °C. This mass loss is due to the burning of carbon though the used carbon is stable up ≤ 400 °C (Shah et al., 2019). Perhaps, the presence of Co_3O_4 decreased burning temperature of the carbon. Besides, Co$(NO_3)_2 \cdot 6H_2O$ could be decomposed to cobalt oxide at ≤ 270 °C as per our earlier report (Ahmed Qasem et al., 2017). This discussion also proves that the selection of 300 °C for preparation of nano-Co_3O_4-C by thermal decomposition of Co$(NO_3)_2 \cdot 6H_2O$ in the presence of home-made carbon was optimal for preserving the carbon.

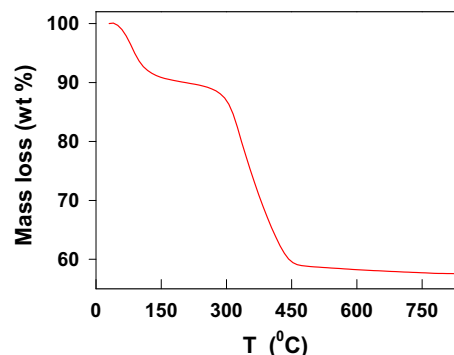**Fig. 6**   (a, b) TEM, (c) HRTEM images and (d) SAED pattern of typical nano-Co_3O_4-C-400.

Fig. 7   TGA spectrum of nano-Co_3O_4-C-400 in air.

3.5. X-ray photoelectron spectroscopy analysis of nano-Co₃O₄-C

The X-ray photoelectron spectroscopy (XPS) measurements were performed to know the chemical information of the prepared nano-Co_3O_4-C-400. The XPS survey scan spectrum of the sample is shown in Fig. 8(A). It indicates four major peaks at around 284.6, 400, 531 and 785 eV. These peaks represent the C1s, N1s, O1s and Co2p core levels, respectively. It clearly shows the presence of Co, O, N, C, and Si. The presence of Co, O, and C is expected. While the presence of Si and N might be due to impurities in carbon that comes from the preparation from natural plant, because the presence of nitrogenous and silicate compounds in plants are very common (Ohyama, 2010; Shah et al., 2019), The high-resolution spectra of C1s, Co2p and O1s were also recorded and presented in Fig. 8(B)–(D), respectively. For a comprehensive evaluation of oxidation states and the chemical environment of each element, the peaks corresponding to C1s, Co2p and O1s were deconvoluted and fitted. Besides, the presence of characteristic XPS peaks for Co2p is related to Co_3O_4. As shown in Fig. 8(C), the XPS spectra for the Co2p of the composite exhibit three peaks at ~781, ~785 eV and ~798 eV attributed to the Co2p$_{3/2}$, Co2p$_{3/2}$ (satellite) and Co2p$_{1/2}$ states of Co_3O_4, respectively. The O1s XPS spectra, shown in Fig. 8 (D) exhibit two deconvoluted components. The component 530.2 eV is ascribed to oxygen atoms in the cobalt particles, while the other component centered at 533.5 eV is related to C—O/O═C—O (Babar et al., 2018; Petitto et al., 2008; Sundar et al., 2016) groups. This gives a further proof of the Co_3O_4-C formation by the thermal decomposition of $Co(NO_3)_2 \cdot 6H_2O$

3.6. Diffuse reflectance spectroscopy of nano-Co₃O₄-C

The direct band gap of nano-Co_3O_4-C-400 was calculated using diffuse reflectance spectroscopy (DRS), that estimated by Tauc's relation (Escobedo Morales et al., 2007) given below (equation (2));

$$[F(R)hv]^2 = C(hv - E_g) \qquad (2)$$

where $F(R)$ is the Kubelka-Munk function, hv is the photon energy, E_g represents the band gap, and C is a proportionality constant. The band gap of nano-Co_3O_4-C-400 was measured from Fig. 9 and was found to be 1.36 eV, which is in good agreement with the previously reported value for Co_3O_4 nanoparticles (Bhargava et al., 2018).

3.7. Fourier Transform Infrared Spectroscopy (FTIR)

Fig. 10 represents the FTIR spectra of the prepared nano-Co_3O_4-C-400 and Co_3O_4 samples. The two sharp peaks at 572 and 661 cm^{-1} in the FTIR spectrum of nano-Co_3O_4-C-400 and Co_3O_4 are related to the stretching vibrations of Co—O (Xu et al., 2015). The presence of these peaks supports the formation of the Co_3O_4 spinel network and are associated with the OB$_3$ (B denotes Co^{3+} in an octahedral hole) and the ABO (A denotes the Co^{2+} in a tetrahedral hole) vibrations in the spinel lattice (Xu et al., 2015). Both nano-Co_3O_4-C-400 and Co_3O_4 have two peaks at 1118. The peak at 1118 cm^{-1} is attributed to the stretching vibrations of C—O (Xu et al., 2015). The sharp and intense peak at 1398 cm^{-1} is appeared
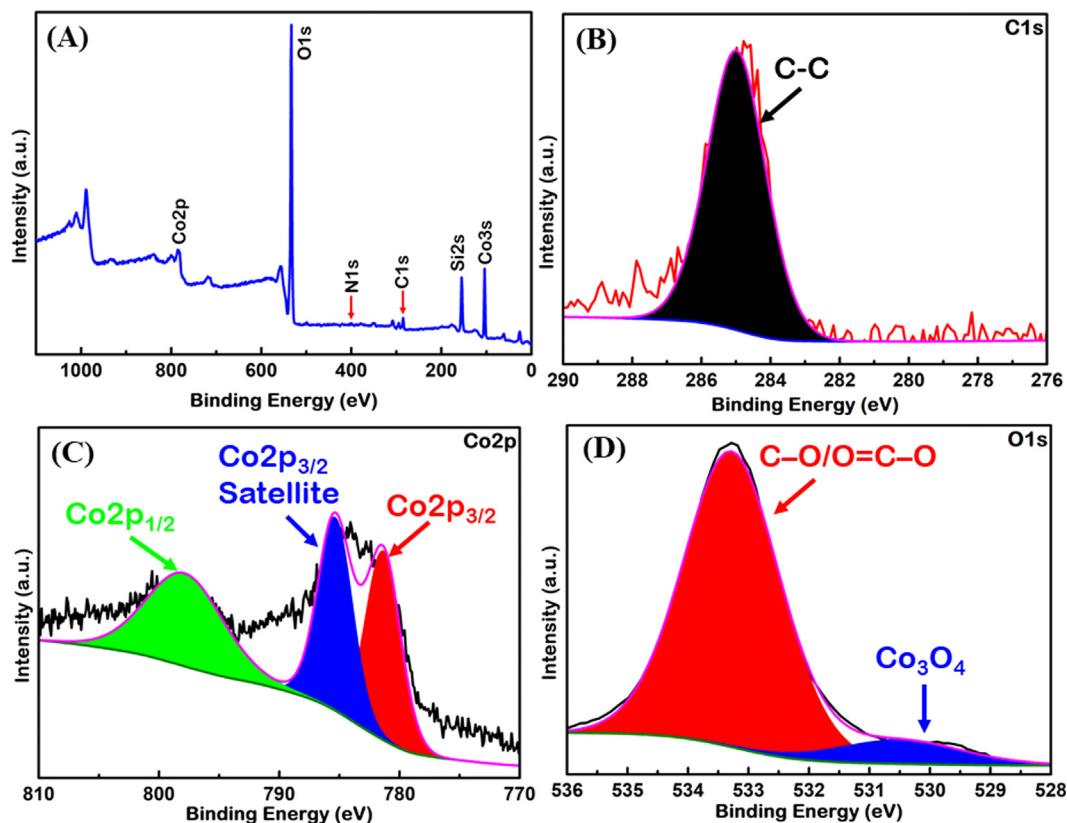

Fig. 8 (A) XPS survey spectrum of nano-Co₃O₄-C-400 with four major peaks of carbon, oxygen, cobalt and nitrogen. The high resolution survey spectra of (B) C1s, (C) Co2p and (D) O1s of nano-Co₃O₄-C-400.
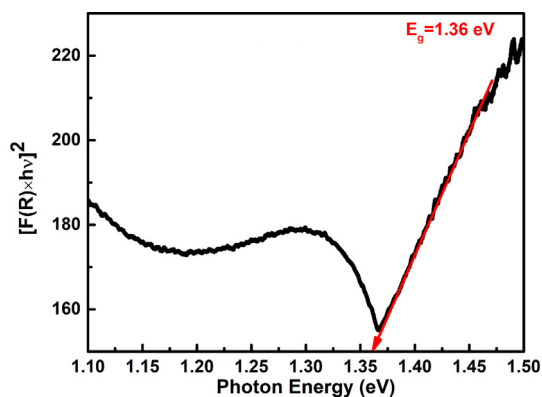
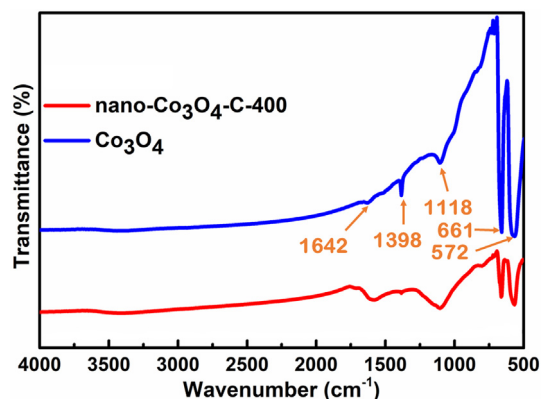**Fig. 9** Thse band gap energy of the prepared nano-Co_3O_4-C-400.

Fig. 10 FTIR spectra of nano-Co_3O_4-C-400 and Co_3O_4.

for Co_3O_4. This peak corresponds to the stretching vibration of NO_3^-, which is due to the residue of $Co(NO_3)_2$ (Xu et al., 2015). However this peak is very minor for the case of nano-Co_3O_4-C-400 i.e. almost all $Co(NO_3)_2$ decomposed to Co_3O_4 in the presence of carbon. The other minor peak at 1642 cm^{-1} in the spectrum of Co_3O_4 may be assigned for molecular water due to the absorbed moisture (Xu et al., 2015). However, the relatively intense peak of nano-Co_3O_4-C-400 at 1642 cm-1 could be related to the C=O bonds in carboxylic acid/C=C of olefinic group/C=N in addition to molecular water peak. These functional group is expected from our prepared carbon. The details related to FTIR of carbon

will be summarized in our next paper with other synthesized carbonaceous materials.

3.8. Brunauer-Emmett-Teller (BET) analysis of nano-Co_3O_4-C-400

Adsorption-desorption isotherm and BJH adsorption pore distribution for nano-Co_3O_4-C-400 are depicted in Fig. 11(A) and (B) respectively. The curve in Fig. 11(A) demonstrates composite Type IV + Type II isotherm i.e. nano-Co_3O_4-C-400 possess both meso- and macropores (Thommes et al., 2015). Fig. 11 (B) presents a wide distribution of pore diameter (Range: 1.93–170 nm) with a BJH adsorption average pore diameter of 9.76 nm. The range of pore diameter, average pore diameter (11(B)) and type of curve (11(A)) also indicate large fractions of mesopores in nano-Co_3O_4-C-400.

3.9. Electrocatalytic activities of nano-Co_3O_4-C

The electrocatalytic activity of nano-Co_3O_4-C was assessed by cyclic voltammetry (CV) in 0.1 M NaOH (aq.) solution (pH 13). In Fig. 12, the cyclic voltammograms (CVs) of the (a) bare carbon/FPCE, (b) nano-Co_3O_4-C-100/FPCE, (c) nano-Co_3O_4-C-200/FPCE, (d) nano-Co_3O_4-C-400/FPCE, (e) nano-Co_3O_4-C-600/FPCE, (f) nano-Co_3O_4-C-800/FPCE, and (g) nano-Co_3O_4-C-1000/FPCE is shown. By comparing the CVs in Fig. 12, carbon/FPCE is the least active for electrochemical water oxidation. The activity of the nano-Co_3O_4-C/FPCE increases with increasing the amount of precursor. The reached current densities for (a) bare carbon/FPCE, (b) nano-Co_3O_4-C-100/FPCE, (c) nano-Co_3O_4-C-200/FPCE and (d) nano-Co_3O_4-C-400/FPCE at 1.5 V are approximately 9.1, 12.5, 17.2 and 28.2 mA cm^{-2}, respectively. Nano-Co_3O_4-C-100, nano-Co_3O_4-C-200, and Co_3O_4-C-400 started to setup oxidation of water at a low potential of 0.7 V; it is obvious that there is a significant improvement toward water oxidation by increasing the amount of cobalt oxide. The current densities for (e) nano-Co_3O_4-C-600/FPCE, (f) nano-Co_3O_4-C-800/ FPCE and (g) nano-Co_3O_4-C-1000/FPCE at 1.5 V are 22.5, 27.1 and 35.1 mA cm^{-2}, respectively. To further evaluate the optimum catalyst, the catalytic properties of the prepared electrodes towards electrochemical water oxidation are compared in Table 2 in terms of current densities at 1.5 V, starting potentials and overpotentials at 5 mA/cm^2 determined from curves shown in Fig. 12.
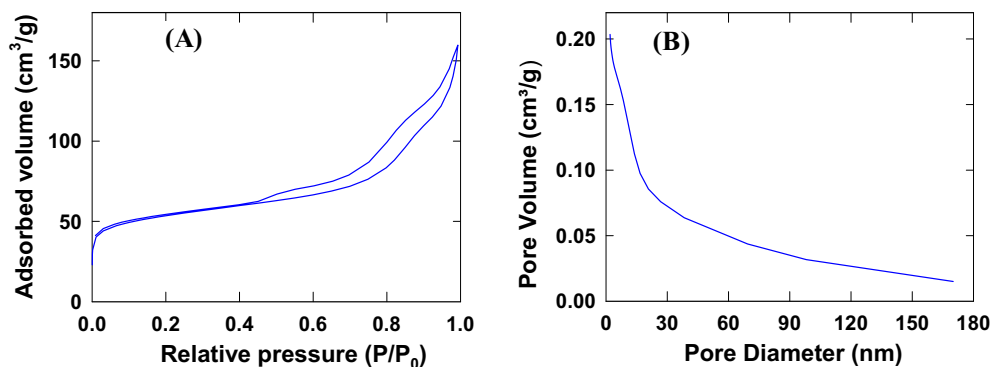

Fig. 11 (a) Nitrogen adsorption-desorption isotherm and (b) Corresponding BJH pore size distribution of nano-Co_3O_4-C-400.

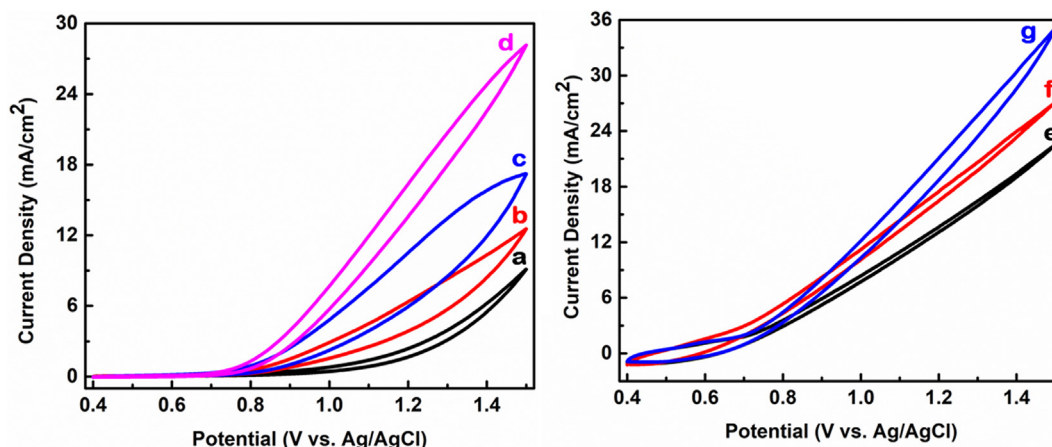**Fig. 12** (a) Cyclic voltammograms of C/FPCE, (b) nano-Co$_3$O$_4$-C-100/FPCE, (c) nano-Co$_3$O$_4$-C-200/FPCE, (d) nano-Co$_3$O$_4$-C-400/FPCE, (e) nano-Co$_3$O$_4$-C-600/FPCE, (f) nano-Co$_3$O$_4$-C-800/FPCE, and (g) nano-Co$_3$O$_4$-C-1000/FPCE in 0.1 M NaOH (aq.). To prepare the modified electrode, 30 μL of 2 mg/ml catalyst solution (aq.) was dropped and dried.

Table 2 Comparison of the prepared electrodes in terms of current densities at 1.5 V, starting potentials, and overpotentials at 5 mA/cm^2 of electrochemical water oxidation.

Types of Electrodes	Current density at 1.5 V (mA/cm^2)	Starting potential for water oxidation (mV vs. Ag/AgCl)	Overpotential at 5 mA/cm^2 (mV vs. Ag/AgCl)
C/FPCE	9.1	700	1351
nano-Co$_3$O$_4$-C-100/FPCE	12.5	700	1290
nano-Co$_3$O$_4$-C-200/FPCE	17.2	700	1007
nano-Co$_3$O$_4$-C-400/FPCE	28.2	700	931
nano-Co$_3$O$_4$-C-600/FPCE	22.5	750	863
nano-Co$_3$O$_4$-C-800/FPCE	27.1	750	788
nano-Co$_3$O$_4$-C-1000/FPCE	35.1	780	817

This work shows that the current densities, at 1.5 V, increases by increasing the amount of cobalt oxide in the prepared samples. The nano-Co$_3$O$_4$-C-400 catalyst shows optimum performance for electrochemical water oxidation in terms of starting water oxidation potential, reasonable amount of Co$_3$O$_4$ and moderate level of current density at 1.5 V. The water oxidation current density of nano-Co$_3$O$_4$-C-400/FPCE

is much higher than that of the electrodeposited MnOx/ITO electrode. That is, nano-Co$_3$O$_4$-C-400/FPCE has higher sensitivity for water oxidation than that of electrodeposited MnO$_x$/ITO electrode (Aziz et al., 2017).

To check the loading effect of the catalyst on the electrode surface, we loaded different amounts of the prepared nano-Co$_3$O$_4$-C-400 on FPCE as described in Fig. 13(A). The data

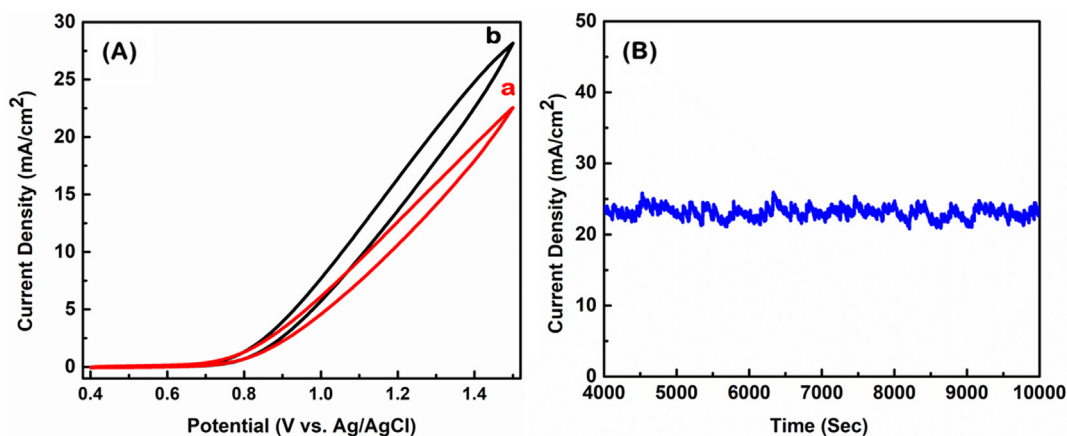**Fig. 13** (A) Cyclic voltammograms of nano-Co$_3$O$_4$-C-400/FPCE in 0.1 M NaOH (aq.), to prepare the modified electrode, 30 μL of (a) 2 mg/ml and (b) 1 mg/ml catalyst solution (aq.) were dropped and dried. (B) Amperogram of nano-Co$_3$O$_4$-C-400/FPCE in 0.1 M NaOH at 1.0 V vs. Ag/AgCl.

revealed that electrocatalytic properties of the nano-Co_3O_4-C-400/FPCE also depend on the loading amount of the nano-Co_3O_4-C-400 on FPCE. The water oxidation potential remains constant and the current density at 1.5 V decreases with the increase in the amount of nano-Co_3O_4-C-400. The stability test of nano-Co_3O_4-C-400/FPCE was carried out in 0.1 M NaOH for 10,000 s (Fig. 13(B)). The electrode demonstrated excellent stability since the current density remained constant throughout the measurement period. This result shows that the prepared catalyst (nano-Co_3O_4-C-400) is capable of sustaining water oxidation and can be utilized for practical applications such as production of H_2 and O_2, and the reduction of CO_2 to valuable fuels.

4. Conclusion

Nano-Co_3O_4) with different morphologies were fabricated on porous carbon prepared from natural products. We demonstrated a facile method for synthesizing nano-Co_3O_4-C, where nano-Co_3O_4 was successfully decorated on home-made *Albizia procera* (Roxb.) based carbon using a straightforward thermal decomposition method. The prepared samples were characterized by XRD, SEM, EDS, TGA, HRTEM, FTIR, BET, DRS and XPS. The XRD data confirmed the formation of Co_3O_4-C nanoparticles with face centered cubic structure. EDS and XPS confirmed the presence of Co, O and C, as expected, in addition to Si and N which probably come from the natural carbon material. The TGA analysis revealed that major mass loss started at 320 °C due to carbon loss. The Co_3O_4-C NPs were immobilized on FPCE for electrochemical measurements. The nano-Co_3O_4-C/FPCE composite shows excellent electrocatalytic properties towards electrochemical water oxidation in 0.1 M NaOH (aq.). It is obtained that the nano-Co_3O_4-C-400/FPCE sample delivers optimum catalytic properties among all the prepared nano-Co_3O_4-C/FPCE catalysts. The nano-Co_3O_4-C-400/FPCE composite shows good stability in water oxidation. The overall electrochemical activity and stability of nano-Co_3O_4-C proved to be excellent and suitable agent for water oxidation. Such high-efficiency of nano-Co_3O_4-C/FPCE should be suitable for other electrochemical applications including production of clean H_2 and O_2 and conversion of CO_2 to fuels.

Declaration of Competing Interest

The authors declared that there is no conflict of interest.

Acknowledgement

References

Ahmed, J., Ahmad, T., Ramanujachary, K.V., Lofland, S.E., Ganguli, A.K., 2008. Development of a microemulsion-based process for synthesis of cobalt (Co) and cobalt oxide (Co_3O_4) nanoparticles from submicrometer rods of cobalt oxalate. J. Colloid Interface Sci. 321, 434–441. https://doi.org/10.1016/j.jcis.2008.01.052.

Ahmed Qasem, M.A., Aziz, M.A., Hakeem, A.S., Onaizi, S.A., 2017. Preparation of nano-Co_3O_4 by direct thermal decomposition of cobalt(II) nitrate hexahydrate for electrochemical water oxidation. Curr. Nanosci. 14. https://doi.org/10.2174/1573413713666171201150215.

Asif, M., Muneer, T., 2007. Energy supply, its demand and security issues for developed and emerging economies. Renew. Sustain. Energy Rev. https://doi.org/10.1016/j.rser.2005.12.004.

Aslan, C., Ilhan, S., Kalpakli, A.O., Kahruman, C., Yusufoglu, I., 2019. Reaction mechanism of strontium cobaltite synthesis from equimolar mixture of $Sr(NO_3)_2$ and $Co(NO_3)_2$ •$6H_2O$ under air atmosphere. Thermochim. Acta 676, 52–63. https://doi.org/10.1016/j.tca.2019.03.030.

Aziz, M.A., El-Madkhoum, A., Hakeem, A.S., Shaikh, M.N., Rehman, A.U., Yamani, Z.H., 2017. Effect of Mn precursors on the morphology and electrocatalytic activity toward water oxidation of micro-nanostructured MnO_x films prepared by voltammetric deposition. J. Mater. Sci. Mater. Electron. 28, 18463–18473. https://doi.org/10.1007/s10854-017-7793-6.

Babar, P.T., Lokhande, A.C., Pawar, B.S., Gang, M.G., Jo, E., Go, C., Suryawanshi, M.P., Pawar, S.M., Kim, J.H., 2018. Electrocatalytic performance evaluation of cobalt hydroxide and cobalt oxide thin films for oxygen evolution reaction. Appl. Surf. Sci. 427, 253–259. https://doi.org/10.1016/j.apsusc.2017.07.142.

Bajdich, M., García-Mota, M., Vojvodic, A., Nørskov, J.K., Bell, A.T., 2013. Theoretical investigation of the activity of cobalt oxides for the electrochemical oxidation of water. J. Am. Chem. Soc. 135, 13521–13530. https://doi.org/10.1021/ja405997s.

Bergmann, A., Martinez-Moreno, E., Teschner, D., Chernev, P., Gliech, M., De Araújo, J.F., Reier, T., Dau, H., Strasser, P., 2015. Reversible amorphization and the catalytically active state of crystalline Co_3O_4 during oxygen evolution. Nat. Commun. 6. https://doi.org/10.1038/ncomms9625.

Bhargava, R., Khan, S., Ahmad, N., Ansari, M.M.N., 2018. Investigation of structural, optical and electrical properties of Co_3O_4 nanoparticles. In: AIP Conference Proceedings. American Institute of Physics Inc.. https://doi.org/10.1063/1.5032369.

Bhattacharjee, C.R., Purkayastha, D.D., Das, N., 2013a. Surfactant-controlled low-temperature thermal decomposition route to monodispersed phase pure tricobalt tetraoxide nanoparticles. Mater. Lett. 90, 111–114. https://doi.org/10.1016/j.matlet.2012.09.031.

Bhattacharjee, C.R., Purkayastha, D.D., Das, N., 2013b. Surfactant-free thermal decomposition route to phase pure tricobalt tetraoxide nanoparticles from cobalt(II)-tartrate complex. J. Sol–Gel Sci. Technol. 65, 296–300. https://doi.org/10.1007/s10971-012-2935-z.

Blakemore, J.D., Crabtree, R.H., Brudvig, G.W., 2015. Molecular catalysts for water oxidation. Chem. Rev. 115, 12974–13005. https://doi.org/10.1021/acs.chemrev.5b00122.

Chen, Z., Kronawitter, C.X., Koel, B.E., 2015. Facet-dependent activity and stability of Co_3O_4 nanocrystals towards the oxygen evolution reaction. Phys. Chem. Chem. Phys. 17, 29387–29393. https://doi.org/10.1039/c5cp02876k.

Chu, S., Majumdar, A., 2012. Opportunities and challenges for a sustainable energy future. Nature. https://doi.org/10.1038/nature11475.

Deng, X., Tüysüz, H., 2014. Cobalt-oxide-based materials as water oxidation catalyst: Recent progress and challenges. ACS Catal. https://doi.org/10.1021/cs500713d.

Diallo, A., Beye, A.C., Doyle, T.B., Park, E., Maaza, M., 2015. Green synthesis of Co_3O_4 nanoparticles via Aspalathus linearis: physical properties. Green Chem. Lett. Rev. https://doi.org/10.1080/17518253.2015.1082646.

Dragunov, V.P., Dorzhiev, V.Y., Ostertak, D.I., Atuchin, V.V., 2018. A new autostabilization mechanism in the Bennet doubler circuit-based electrostatic vibrational energy harvester. Sens. Actuators, A Phys. 272, 259–266. https://doi.org/10.1016/j.sna.2018.01.053.

Escobedo Morales, A., Sánchez Mora, E., Pal, U., Escobedo Morales, A., Sánchez Mora, E., Pal, U., 2007. Use of diffuse reflectance spectroscopy for optical characterization of un-supported nanostructures. RMxFS 53, 18–22.

Fernández-García, M., Martínez-Arias, A., Hanson, J.C., Rodriguez, J.A., 2004. Nanostructured oxides in chemistry: characterization and properties. Chem. Rev. 104, 4063–4104. https://doi.org/10.1021/cr030032f.

Gerken, J.B., McAlpin, J.G., Chen, J.Y.C., Rigsby, M.L., Casey, W.H., Britt, R.D., Stahl, S.S., 2011. Electrochemical water oxidation with cobalt-based electrocatalysts from pH 0–14: The thermodynamic basis for catalyst structure, stability, and activity. J. Am. Chem. Soc. 133, 14431–14442. https://doi.org/10.1021/ja205647m.

Guo, C., Zhang, X., Huo, H., Xu, C., Han, X., 2013. Co$_3$O$_4$ microspheres with free-standing nanofibers for high performance non-enzymatic glucose sensor. Analyst 138, 6727–6731. https://doi.org/10.1039/c3an01403g.

Harish, S., Silambarasan, K., Kalaiyarasan, G., Narendra Kumar, A.V., Joseph, J., 2016. Nanostructured porous cobalt oxide synthesis from Co$_3$[Co(CN)$_6$]$_2$ and its possible applications in Lithium battery. Mater. Lett. https://doi.org/10.1016/j.matlet.2015.11.122.

Hunter, B.M., Gray, H.B., Müller, A.M., 2016. Earth-abundant heterogeneous water oxidation catalysts. Chem. Rev. https://doi.org/10.1021/acs.chemrev.6b00398.

Jia, W., Guo, M., Zheng, Z., Yu, T., Rodriguez, E.G., Wang, Y., Lei, Y., 2009. Electrocatalytic oxidation and reduction of H$_2$O$_2$ on vertically aligned Co$_3$O$_4$ nanowalls electrode: toward H$_2$O$_2$ detection. J. Electroanal. Chem. 625, 27–32. https://doi.org/10.1016/j.jelechem.2008.09.020.

Jiao, Y., Zheng, Y., Jaroniec, M., Qiao, S.Z., 2015. Design of electrocatalysts for oxygen- and hydrogen-involving energy conversion reactions. Chem. Soc. Rev. https://doi.org/10.1039/c4cs00470a.

Kabre, T.S., Program, G., Chemistry, I., 2011. Co$_3$O$_4$ Thin Films: Sol-Gel Synthesis, Electrocatalytic Properties; Photoelectrochemistry. The Ohio State University.

Kanan, M.W., Nocera, D.G., 2008. In situ formation of an water containing phosphate and Co^{2+}. Science 321, 1072–1075. https://doi.org/10.1126/science.1162018.

Kang, M., Zhou, H., 2015. Facile synthesis and structural characterization of Co$_3$O$_4$ nanocubes. AIMS Mater. Sci. 2, 16–27. https://doi.org/10.3934/matersci.2015.1.16.

Khomane, R.B., Agrawal, A.C., Kulkarni, B.D., Gopukumar, S., Sivashanmugam, A., 2008. Preparation and electrochemical characterization of lithium cobalt oxide nanoparticles by modified sol-gel method. Mater. Res. Bull. 43, 2497–2503. https://doi.org/10.1016/j.materresbull.2007.08.033.

Liang, Y., Wang, H., Zhou, J., Li, Y., Wang, J., Regier, T., Dai, H., 2012. Covalent hybrid of spinel manganese-cobalt oxide and graphene as advanced oxygen reduction electrocatalysts. J. Am. Chem. Soc. 134, 3517–3523. https://doi.org/10.1021/ja210924t.

Luisetto, I., Pepe, F., Bemporad, E., 2008. Preparation and characterization of nano cobalt oxide. J. Nanopart. Res. 10, 59–67. https://doi.org/10.1007/s11051-008-9365-4.

Ma, Z., 2014. Cobalt oxide catalysts for environmental remediation. Curr. Catal. 3, 15–26.

Mahmoud, W.E., Al-Agel, F.A., 2011. A novel strategy to synthesize cobalt hydroxide and Co$_3$O$_4$ nanowires. J. Phys. Chem. Solids 72, 904–907. https://doi.org/10.1016/j.jpcs.2011.04.014.

McCrory, C.C.L., Jung, S., Peters, J.C., Jaramillo, T.F., 2013. Benchmarking heterogeneous electrocatalysts for the oxygen evolution reaction. J. Am. Chem. Soc. 135, 16977–16987. https://doi.org/10.1021/ja407115p.

Ohyama, T., 2010. Nitrogen as a major essential element of plants. Nitrogen Assimilation in Plants. Signpost, Trivandrum, Kerala, India.

Petitto, S.C., Marsh, E.M., Carson, G.A., Langell, M.A., 2008. Cobalt oxide surface chemistry: The interaction of CoO(1 0 0), Co$_3$O$_4$(1 1

0) and Co$_3$O$_4$(1 1 1) with oxygen and water. J. Mol. Catal. A Chem. 281, 49–58. https://doi.org/10.1016/j.molcata.2007.08.023.

Qasem, M.A.A., Khan, A., Onaizi, S.A., Mohamed, H.D., Helal, A., Aziz, M.A., 2019. Effect of Co(NO$_3$)$_2$·6H$_2$O thermal decomposition temperature on the nano-Co$_3$O$_4$ product morphology and electrocatalysis of water oxidation. J. Appl. Electrochem. 49, 251–259. https://doi.org/10.1007/s10800-018-1275-2.

Raman, V., Suresh, S., Savarimuthu, P.A., Raman, T., Tsatsakis, A.M., Golokhvast, K.S., Vadivel, V.K., 2016. Synthesis of Co$_3$O$_4$ nanoparticles with block and sphere morphology, and investigation into the influence of morphology on biological toxicity. Exp. Ther. Med. 11, 553–560. https://doi.org/10.3892/etm.2015.2946.

Reier, T., Oezaslan, M., Strasser, P., 2012. Electrocatalytic oxygen evolution reaction (OER) on Ru, Ir, and pt catalysts: a comparative study of nanoparticles and bulk materials. ACS Catal. 2, 1765–1772. https://doi.org/10.1021/cs3003098.

Roger, I., Shipman, M.A., Symes, M.D., 2017. Earth-abundant catalysts for electrochemical and photoelectrochemical water splitting. Nat. Rev. Chem. https://doi.org/10.1038/s41570-016-0003.

Shah, S.S., Aziz, M.A., Mohamedkhair, A.K., Qasem, M.A.A., Hakeem, A.S., Nazal, M.K., Yamani, Z.H., 2019. Preparation and characterization of manganese oxide nanoparticles-coated Albizia procera derived carbon for electrochemical water oxidation. J. Mater. Sci. Mater. Electron. https://doi.org/10.1007/s10854-019-01979-6.

Sharma, J.K., Srivastava, P., Singh, G., Akhtar, M.S., Ameen, S., 2015. Green synthesis of Co$_3$O$_4$ nanoparticles and their applications in thermal decomposition of ammonium perchlorate and dye-sensitized solar cells. Mater. Sci. Eng. B Solid-State Mater. Adv. Technol. 193, 181–188. https://doi.org/10.1016/j.mseb.2014.12.012.

Su, D., Xie, X., Munroe, P., Dou, S., Wang, G., 2014. Mesoporous hexagonal Co$_3$O$_4$ for high performance lithium ion batteries. Sci. Rep. 4. https://doi.org/10.1038/srep06519.

Sundar, L.S., Irurueta, G.O., Venkata Ramana, E., Singh, M.K., Sousa, A.C.M., 2016. Thermal conductivity and viscosity of hybrid nanfluids prepared with magnetic nanodiamond-cobalt oxide (ND-Co$_3$O$_4$) nanocomposite. Case Stud. Therm. Eng. 7, 66–77. https://doi.org/10.1016/j.csite.2016.03.001.

Thommes, M., Kaneko, K., Neimark, A.V., Olivier, J.P., Rodriguez-Reinoso, F., Rouquerol, J., Sing, K.S.W., 2015. Physisorption of gases, with special reference to the evaluation of surface area and pore size distribution (IUPAC Technical Report). Pure Appl. Chem. 87, 1051–1069. https://doi.org/10.1515/pac-2014-1117.

Turner, J.A., 1999. A realizable renewable energy future. Science (80-.). https://doi.org/10.1126/science.285.5428.687.

Wang, J., Cui, W., Liu, Q., Xing, Z., Asiri, A.M., Sun, X., 2016a. Recent progress in cobalt-based heterogeneous catalysts for electrochemical water splitting. Adv. Mater. 28, 215–230. https://doi.org/10.1002/adma.201502696.

Wang, X., Wu, X., Xu, B., Hua, T., 2016b. Coralloid and hierarchical Co$_3$O$_4$ nanostructures used as supercapacitors with good cycling stability. J. Solid State Electrochem. 20, 1303–1309. https://doi.org/10.1007/s10008-016-3125-7.

Wu, J., Xue, Y., Yan, X., Yan, W., Cheng, Q., Xie, Y., 2012. Co$_3$O$_4$ nanocrystals on single-walled carbon nanotubes as a highly efficient oxygen-evolving catalyst. Nano Res. 5, 521–530. https://doi.org/10.1007/s12274-012-0237-y.

Xu, H., Hai, Z., Diwu, J., Zhang, Q., Gao, L., Cui, D., Zang, J., Liu, J., Xue, C., 2015. Synthesis and microwave absorption properties of core-shell structured Co$_3$O$_4$-PANI nanocomposites. J. Nanomater. 2015. https://doi.org/10.1155/2015/845983.

Xu, J.M., Cheng, J.P., 2016. The advances of Co$_3$O$_4$ as gas sensing materials: a review. J. Alloys Compd. https://doi.org/10.1016/j.jallcom.2016.06.086.

Xu, R., Zeng, H.C., 2003. Dimensional control of cobalt-hydroxide-carbonate nanorods and their thermal conversion to one-dimensional arrays of Co$_3$O$_4$ nanoparticles. J. Phys. Chem. B 107, 12643–12649. https://doi.org/10.1021/jp035751c.

Yu, X.Y., Meng, Q.Q., Luo, T., Jia, Y., Sun, B., Li, Q.X., Liu, J.H., Huang, X.J., 2013. Facet-dependent electrochemical properties of Co_3O_4 nanocrystals toward heavy metal ions. Sci. Rep. 3. https://doi.org/10.1038/srep02886.

Zhang, B., Zheng, X., Voznyy, O., Comin, R., Bajdich, M., García-Melchor, M., Han, L., Xu, J., Liu, M., Zheng, L., De Arquer, F.P.G., Dinh, C.T., Fan, F., Yuan, M., Yassitepe, E., Chen, N., Regier, T., Liu, P., Li, Y., De Luna, P., Janmohamed, A., Xin, H.L., Yang, H., Vojvodic, A., Sargent, E.H., 2016. Homogeneously dispersed multimetal oxygen-evolving catalysts. Science (80-.) 352, 333–337. https://doi.org/10.1126/science.aaf1525.

Zhou, S., Wang, G., Xie, Y., Wang, H., Bai, J., 2013. Synthesis of carbon-coated Co_3O_4 composite with dendrite-like morphology and its electrochemical performance for lithium-ion batteries. J. Nanopart. Res. 15. https://doi.org/10.1007/s11051-013-1740-0.

Zotov, L.G., Razinkin, V.P., Atuchin, V.V., 2017. Controllable electronic transformer based on the resonance structure with switching capacitor for low-rise buildings residential area power supply stabilization systems. Int. J. Electr. Power Energy Syst. 91, 117–120. https://doi.org/10.1016/j.ijepes.2017.03.004.

Zsigmondy, R., Scherrer, P., 1912. Bestimmung der inneren Struktur und der Größe von Kolloidteilchen mittels Röntgenstrahlen. In: Kolloidchemie Ein Lehrbuch. Springer Berlin Heidelberg, pp. 387–409. https://doi.org/10.1007/978-3-662-33915-2_7.

Züttel, A., Remhof, A., Borgschulte, A., Friedrichs, O., 2010. Hydrogen: The future energy carrier. Philos. Trans. R. Soc. A Math. Phys. Eng. Sci. https://doi.org/10.1098/rsta.2010.0113.